ORIGINAL PAPER

ARCHAEOMETRIC ANALYSES ON PRECUCUTENI-TYPE POTTERY FROM TRANSYLVANIA (ROMANIA). CASE STUDY: ALBA IULIA-*LUMEA NOUĂ*

DIANA ELENA TOMUS (SZABO)[1], MIHAI GLIGOR[1], IOANA DANIELA DULAMA[2*], CRISTIANA RADULESCU[2,3*], IOAN ALIN BUCURICA[2*], SORINA GEANINA STANESCU[2], RALUCA MARIA STIRBESCU[2]

Manuscript received: 20.11.2020; Accepted paper: 12.02.2021; Published online: 30.03.2021.

Abstract: *The aim of this paper is to find out - for the first time - through archaeometric analysis the provenance of the Precucuteni-type pottery from Alba Iulia-Lumea Nouă settlement and whether it has a local origin or is an imported ceramic. The presence of so-called Precucuteni-type pottery in Transylvanian sites, decorated by motifs using excision techniques, represents one of the most challenging debates related to the understanding of the material culture that belongs to Early Eneolithic human communities in the Intra-Carpathian area. A combination of non-invasive / micro-destructive analytical techniques and statistical methods were applied to provide comprehensive information about the studied fragments. In this respect, ten pottery samples were investigated to establish the elemental and molecular composition, as well as its origin. Overall, the analytical and statistical analyses show us that the local production of pottery is predominant, with a limited presence of imports. In summary, nine ceramic fragments out of all analyzed samples belong to the same group, with a strong correlation between them, confirming that they are locally made, while one sample can be considered as imported from elsewhere or obtained through mixing clay with some existing soils in the area during the pottery production stage.*

Keywords: *Precucuteni-type pottery; Early Eneolithic; Alba Iulia-Lumea Nouă archaeological site; firing temperature; clay source; statistical analysis.*

1. INTRODUCTION

Nowadays, it is widely accepted by scientists that the Precucuteni culture originated in the central-western part of Moldova and in south-eastern Transylvania [1, 2] under the influence of Boian and LBK (Linear Band Keramik in German language, which is equivalent to Linear Pottery Culture) cultures. Based on archaeological investigation, it was observed that at the end of the first culture phase, the Precucuteni communities reached the center of Transylvania, were assimilated by the bearers of local cultures and lost their cultural identity [3]. This hypothesis is also supported by the lack of Precucuteni phase III materials in the sites from Transylvania [3]. At this point, the Precucuteni-type ceramic discovered in Transylvania's archaeological sites is considered as imports by some specialists [4], and by

[1] 1 Decembrie 1918 University of Alba Iulia, 510009 Alba Iulia, Romania.
E-mail: diana-elena.tomus@uab.ro; mihai.gligor@uab.ro.
[2] Valahia University of Targoviste, Institute of Multidisciplinary Research for Science and Technology, 130004 Targoviste, Romania. E-mail: geaninastanescu@yahoo.com; stirbescu_nic@yahoo.com.
[3] Valahia University of Targoviste, Faculty of Sciences and Arts, 130004 Targoviste, Romania.
[*] *Corresponding authors:* dulama_id@yahoo.com; bucurica_alin@yahoo.com; radulescucristiana@yahoo.com.

others they are interpreted as a fashion of decorating pottery during the Early Eneolithic period (4600-4400 BC) [5-7].

At the present, there are at least 37 archeological sites in Transylvania, where discovered Precucuteni-type ceramic materials [5, 6]. Relevant archaeological research for this topic has been done in the past decades at Alba Iulia-Lumea Nouă, one of the most important sites from the middle Mureș Valley. The settlement of Alba Iulia - Lumea Nouă is located in the N-E part of the city (46°5'3.2748" N, 23°34'4.494" E – Fig. 1).

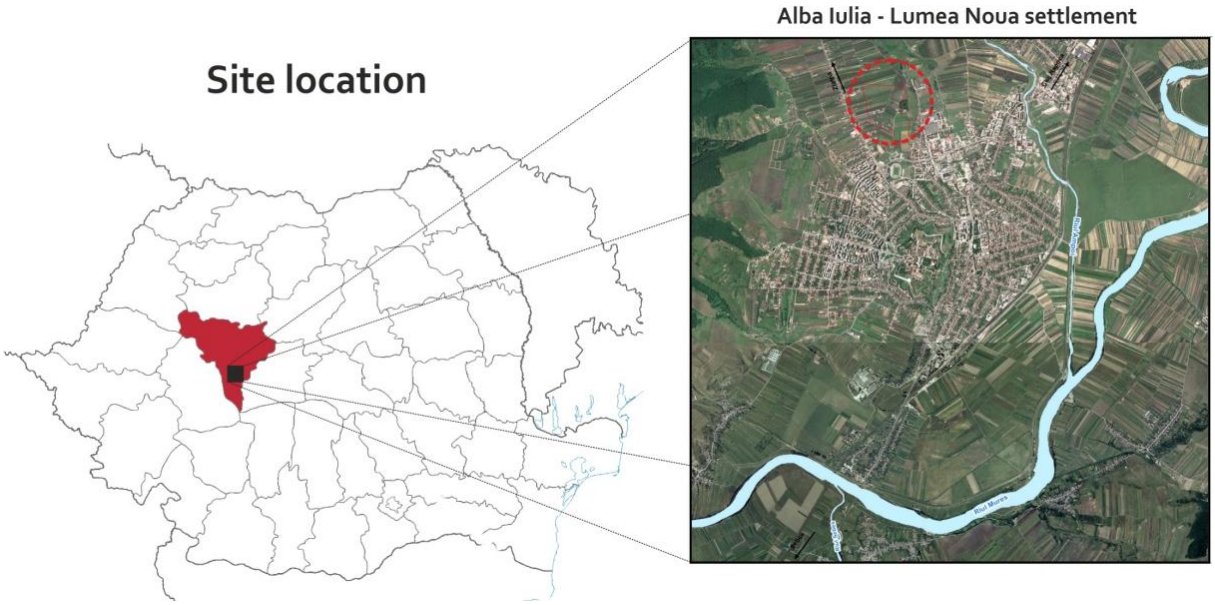

Figure 1. Alba Iulia - Lumea Nouă archaeological site.

Since 1942, several archeological campaigns have been carried out, both preventive and systematic [7]. The site is divided into 3 areas: zone A, where the earliest Vinča B1-B2 materials were discovered, Lumea Nouă painted pottery, Foeni, Precucuteni-type and Petrești pottery; zone B, here a late Vinča B2 / C pottery, Lumea Nouă painted pottery, and Petrești ceramic was discovered; and area C, which includes an intense Foeni habitation, with Turdaș and Precucuteni-type materials [7]. The Precucuteni-type pottery discovered at the Lumea Nouă site presents a fabric, firing and polishing techniques which are typically of the Foeni pottery excavated from Foeni features [7]. The identification of Precucuteni-type decoration, on Foeni vessels, in Foeni features and the lack of Precucuteni habitation levels in the site from Alba Iulia-Lumea Nouă and in other settlements from Transylvania, especially from the middle Mureș Valley, can indicate a fashion of ceramics decoration [5]. There was a question mark about this type of pottery decoration and about the hypothesis that not all the Precucuteni-type ceramic should be considered an import, but a local production ceramic [6].

In order to understand whether the Precucuteni-type pottery has a local origin or is an imported ceramic, this study aims to find out – for the first time – its provenance through archaeometric analysis. Morphological and chemical analyses were used to predict the firing temperature, to evaluate the Pearson's correlations between chemical elements, to analyze the similarity relationship between pottery and clay, as well as to establish the clay source of pottery.

2. MATERIALS AND METHODS

2.1. OBJECTS DESCRIPTION

The Precucuteni-type pottery discovered in the Alba Iulia-Lumea Nouă site can be included in the repertoire of ornaments tipical of phases I and II of the Precucuteni culture [3] – which are 'wolf's teeth' and 'chessboard' [6]. The decoration is executed inside the incised parallel lines using the excision technique and consists in the 'wolf 's teeth' and 'chessboard' ornamental motifs (Fig. 2a).

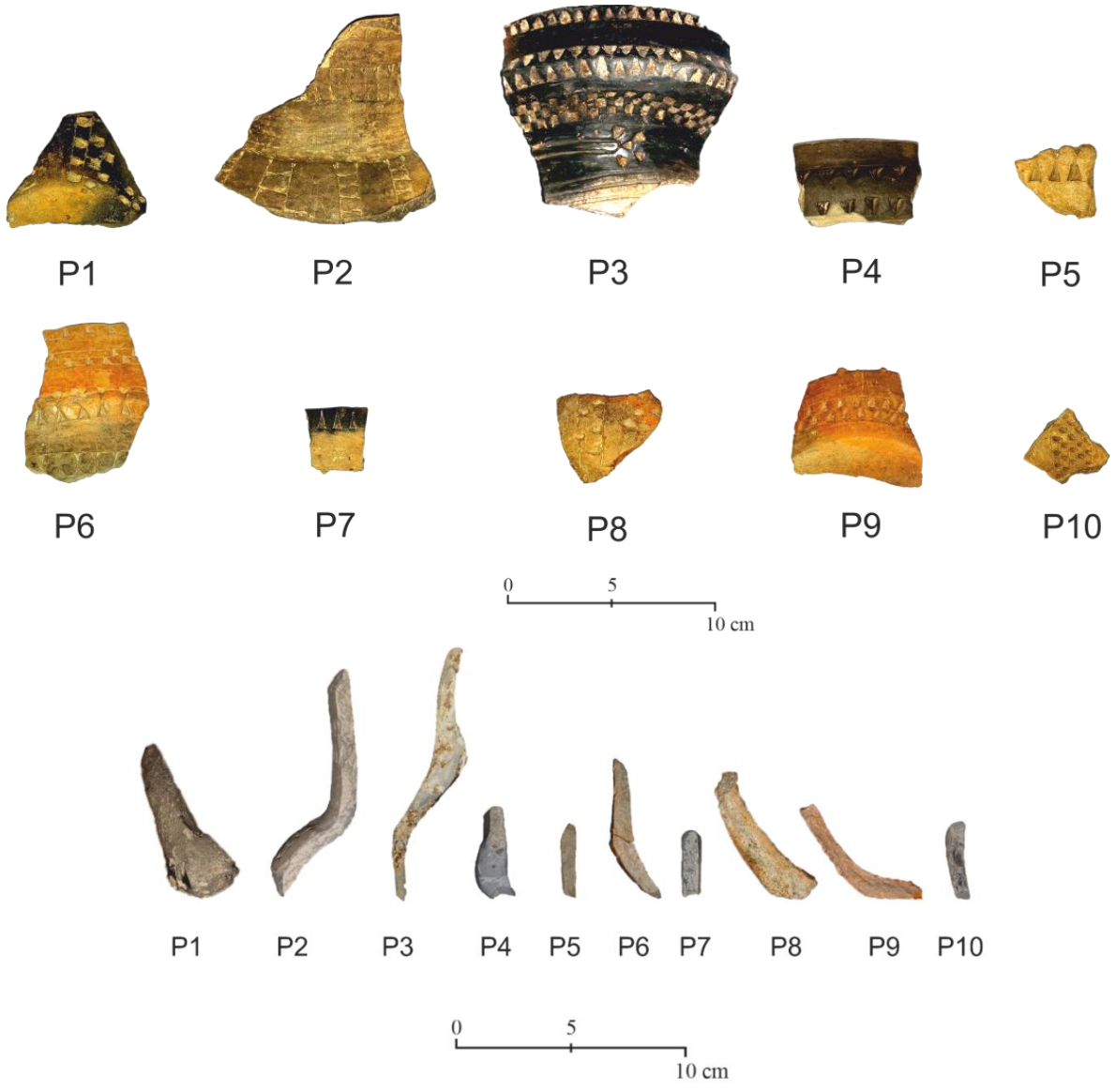

Figure 2. Precucuteni-type pottery from Alba Iulia-Lumea Nouă archaeological site: a) general view; b) edge section of the samples.

Both the triangles and the squares are sometimes arranged in bands, each composed of two alternating rows bordered by incised lines. Within the decoration of the same vessel we encounter a combination of the 'wolf 's teeth' and 'chessboard' motifs. In the first phase of

the Precucuteni culture, in sites from Moldova area, the 'apex' motif [3, 8] appears, having its origin in degenerate Notenkopfkeramik from the LBK culture. This type of decoration is also used in the second phase of the culture [3], but less frequently.

Until now, in Transylvanian sites, the 'apex' ornament has been a very rarely identified motif on the Precucuteni-type ceramic. Only 3 ceramic pieces were known to have been discovered in Turdaș [9], but in 2018 another vessel was discovered at Lumea Nouă site, which was ornamented with 'wolf's teeth', 'chessboard' and 'apex' and its excisions were filled with white paste (Fig. 2; P3), which is common for the Precucuteni phase I from Moldova area [3, 8]. In the first phase of the Precucuteni culture, in the Eastern Romanian territory especially, decorations such as 'wolfs' teeth' and 'chessboard' are predominant, which continues in the second phase but gradually degenerate into simple notches [3].

In 2017, 6 clay samples [10] were analyzed along with 10 samples of middle Neolithic Lumea Nouă painted pottery in order to determine the local provenance of the ceramic. Two of the samples were taken from outside the site, C1 - comes from Bărăbanț (Alba Iulia); C2- from Limba (Ciugud Village), and C3, C4, C5, and C6 comes from the Lumea Nouă site and were excavated from an average depth of 1 meter.

The Precucuteni-type ceramic samples from Alba Iulia–Lumea Nouă site belong to vessels excavated between 2006 and 2019 [5, 7] and the archaeological context together with physical and archaeological characteristics are presented in Table 1.

Table 1. Precucuteni Pottery samples – location and description.

Sample code	Archaeological context*	Physical and archaeological characteristics
P1	ALN.I.18; □ F; ↓ 1,63-2,08 m; Cx. 006a	Vessel bottom fragment, fine texture, excized decoration, 'chessboard' ornament
P2	ALN. IV.06; □ 1 ↓1,40 m	Vessel rim fragment, fine texture, excized decoration, 'wolf teeth' ornament
P3	ALN.II.18; □ A ↓ 2,96 m; Cx. 002	Vessel rim fragment, fine texture, excized decoration, 'wolf teeth', 'chessboard' and 'apex' ornaments; excisions filled with white paste
P4	ALN.II.14; □ B ↓ 0,30-0,60 m	Vessel rim fragment, semi-fine texture, excized decoration, 'wolf teeth' ornament
P5	ALN.I.19; □ A ↓ 0,25-0,65 m; Cx. 002	Vessel fragment, semi-fine texture, excized decoration, 'wolf teeth' ornament
P6	ALN.I.06; □ 1 ↓ 0,65-0,85 m; Cx. 001	Vessel rim fragment, semi-fine texture, excized decoration, 'wolf teeth' ornament
P7	ALN.III.14; □ B ↓ 0,80-1,00 m;	Vessel rim fragment, fine texture, excized decoration, 'wolf teeth' ornament
P8	ALN.I.08; □ A ↓ 0,70-0,80 m; Cx. 001	Vessel fragment, semi-fine texture, excized decoration, 'wolf teeth' ornament
P9	ALN.I.11; □ D ↓ 1,50-1,70 m; Cx. 002	Vessel bottom fragment, semi-fine texture, excized decoration, 'wolf teeth' ornament
P10	ALN.II.15; □ B ↓ 1,04-1,14 m; Cx. 002	Vessel rim fragment, semi-fine texture, excized decoration, 'wolf teeth' and 'chessboard' ornaments

*ALN-Alba Iulia-Lumea Nouă; 18 - year of excavation (2018); I. - the number of the trench; □ - square; ↓- depth; Cx. – feature

The fragments represent various types of vessels –bottoms (Fig. 2a-b; P1, P8-P9), rims (Fig. 2a; P2-P4, P7), the neck of an amphora (Fig. 2 a-b; P2), a fragment from a carinated bowl with rounded carina, which is typical for the Foeni group (Fig. 2 a-b; P4), a fragment

from a biconical bowl (Fig. 2 a-b; P6) and body fragments (Fig. 2 a-b; P5, P10). The brick red-greyish semi-fine ceramic predominates (Fig. 2a; P5-P6, P8-10). One ceramic fragment is black, very well burnished, metallic-like pottery belonging to the fine ware category (Fig. 2a; P3), another black one, also belonging to the semi-fine category (Fig. 2a; P4). Black-topped technique is also present in one case (Fig. 2a; P7). Generally, the walls of the vessels are thin and resonant.

For chemical analyses (i.e., EDS and FTIR), about 500 mg from each edge surface of the samples (Fig. 2b) were collected using a plastic scalpel. This sampling mode was chose due to the fact that it is a minimally invasive technique and the original samples are not dameged, as well as, the soil influence (i.e. chemical composition) is much lower on the edge surface than on the faces of the pottery fragment.

2.2. ANALYTICAL TECHNIQUES

In the field of cultural heritage analyses, the analytical techniques applied in each study must be selected as a function of the sample nature, as well as the destructive or nondestructive character of the equipment. The most commonly used techniques in the study of the samples from cultural heritage are: scanning electron microscopy coupled with energy dispersive X-ray spectrometry (SEM-EDS) [10-19], X-ray fluorescence [13, 16, 17, 20], X-ray diffraction (XRD) [11-13, 19], Raman spectroscopy [11-13, 16, 21-23], Fourier transform infrared spectroscopy (FTIR) [10-12, 14-16, 18, 19], X-ray photoelectron spectroscopy (XPS) [24, 25], Auger electron spectroscopy [17, 25], neutron diffraction [20, 26], neutron tomography [13, 27], neutron activation analysis (NAA) [20, 26], and optical microscopy (OM) [12, 13], as nondestructive or minimally invasive techniques. In this study, a combination of few techniques (i.e., OM, SEM-EDS, ATR-FTIR, and Raman spectroscopy) was applied to provide comprehensive information about the studied fragments.

2.2.1. Optical Microscopy (OM)

The samples were observed using Primo Star and Stemi 2000-c optical microscopes equipped with Axiocam 105 digital camera. The magnification varied from ×10 to ×100 depending on the size of the samples. Optical microscopy was used to study the incisions and topography of the pottery, including the surface and in section characteristics of the samples.

2.2.2. Field Emission Scanning Electron Microscopy coupled with Energy Dispersive X-Ray Spectrometry (FE-SEM-EDS)

The morphological investigations were performed using the SU-70 microscope (Hitachi, Ibaraki, Japan). This is a Field Emission (FE-SEM) type which operates under high vacuum (10^{-8} Pa) and allows obtaining high resolution (i.e., 1 nm at 15 kV acceleration voltages). The SEM is coupled with UltraDry (Thermo Fisher Scientific, Waltham – Massachusetts, United States of America) detector for energy dispersive X-ray spectrometry (EDS). The SEM images were obtain using 5 kV acceleration voltage and different values for working distance (i.e., 17.6-18.7 mm), depending on the characteristics of the sample. The determination of the elemental composition was carried out at an acceleration voltage of 10 kV using the Phi-Rho-Z correction method available in NSS software (Version 3.0).

2.2.3. Attenuated Total Reflection - Fourier Transform Infrared Spectroscopy (ATR-FTIR)

Fourier transform infrared spectroscopy (FTIR) was carried out using spectrometer VERTEX 80v (Bruker, Ettlingen, Germany), equipped with an attenuated total reflection (ATR) sample stage and a Hyperion® microscope. The spectra were recorded in transmittance mode and obtained in the mid-IR region of 3000-400 cm^{-1} (0.2 cm^{-1} spectral resolution and 0.1% T accuracy); 32 scans were averaged in order to obtain clear transmittance spectra of each sample. In addition, using a diamond micro-ATR crystal (index of refraction 2.418) on IR spectrometer it was possible to record a high-quality spectra of ceramics sample in the far-IR region of 550–230 cm^{-1}. Spectrometer is protected continuous from atmospheric moisture by constantly purged with dry air. The measurements were achieved only on the edge of ceramic in terms of purity of original material, not from the external surface of sample (Fig. 2b and Subsection 2.1. Objects description). In this respect, each sample piece was placed on the ATR crystal and finally, a pressure equivalent to 0.5-3.0 kg (i.e., force from 4.9 to 29.4 N) was applied. This pressure has been increased gradually, while monitoring the spectrum appearance. Finally, by respecting these requirements a sufficient intensity is reached and the spectrum is scanned. It is well known that, at too low pressure the contact between the sample and the ATR crystal is not sufficient and can lead to a low intensity of the spectrum (i.e., undesired situation) [15, 28, 29]. ATR-FTIR technique requires a small quantity of sample (i.e., about 0.5 mg) which is rapidly analyzed without any further preparation. FTIR is mainly used to identify the unknown compounds by molecular fingerprint (it measuring how much light is absorbed by the bonds of vibrating molecules), but can also be used for estimate the firing temperature of pottery samples [15, 18, 19].

2.2.4. Raman Spectroscopy

Raman spectroscopy, currently a complementary technique for FTIR spectroscopy, is considered a useful tool in the study of cultural heritage artifacts [21, 23]. It allows a rapid identification of the compounds at the micrometer scale without preparing the samples. Raman spectra of the pottery samples were recorded using a portable Xantus-2^{TM} Raman analyzer (Rigaku, Boston, United States of America) equipped with two laser sources (i.e., 785 nm and 1064 nm) and two detectors (i.e., TE cooled CCD and TE cooled InGaAs), which is capable to reduce intrinsic fluorescence issues. A 785 nm laser line was used for excitation and was focused on the different areas of the sample fragments (3-5 scans/spectra). In addition, to avoid changes in the materials due to overheating, neutral density filters were used to set the laser power at the sample to values between 0.2 and 1.0 mW. A 1200 lines/mm grating was used, and integration times were set between 10 and 300 s. The spectral range was 200-2000 cm^{-1}, with 15-18 cm^{-1} spectral resolution.

2.3. Data Processing

The statistical analyses were performed using Microsoft Office Excel (Version 2010) and IBM SPSS Statistics (Version 21). In this regards, average values and standard deviation were determined using Microsoft Office Excel, and principal component analysis (PCA), cluster analysis, as well as Pearson' correlation were performed using IBM SPSS Statistics. Principal component analysis and cluster analysis were used to evaluate the chemical similarities between ceramic fragments and clays [10, 30], while Pearson' correlation were applied for determining differences ($p < 0.05$) in the elemental concentrations of ceramic fragments [31-33].

3. RESULTS

3.1. MORPHOLOGY OF THE CERAMIC FRAGMENTS

The OM image of the P1 sample taken on the external surface (Fig. 3a) reveals an uniform and porous black matrix with fine grains, as well as some parallel rectangular excisions, with straight edges (Fig. 3b). On the surface of these excisions, some beige-brown deposits were observed. The morphology of P1 sample is characterized by fine grains with round edges, with few granular or straight edges inclusions (Fig. 3c-d).

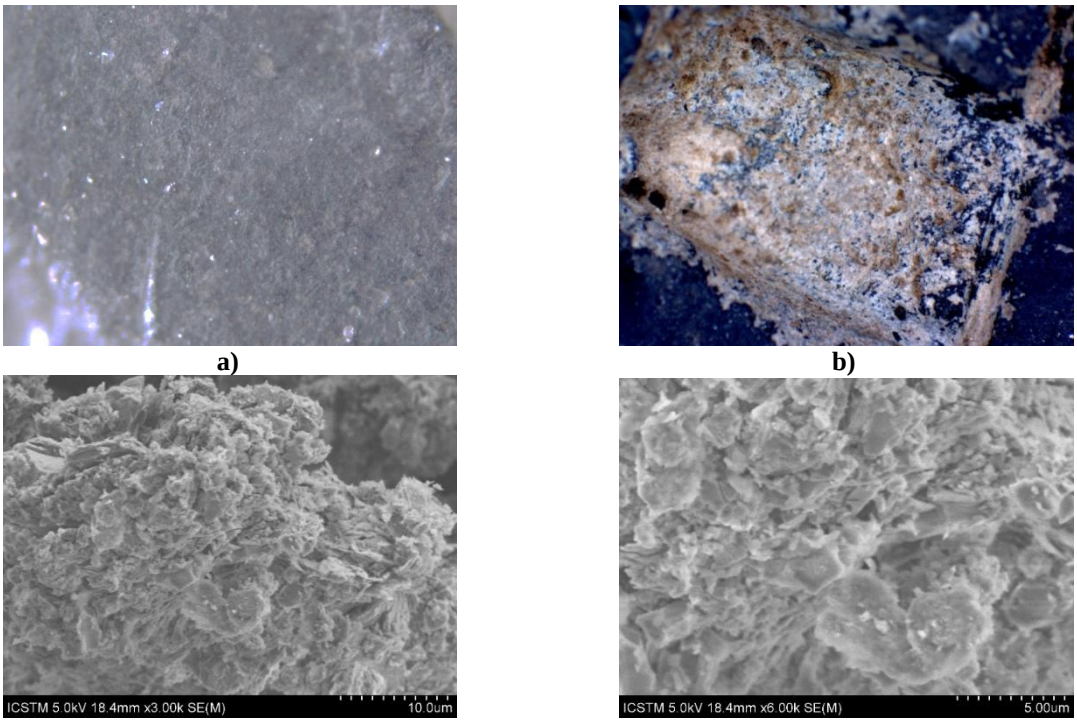

a) **b)** **c)** **d)**

Figure 3. Ceramic sample P1: a) OM of ceramic fragment (x100); b) OM image of excision (x10); c) SEM image of ceramic in the cross section (x3.00k); d) SEM image of ceramic in the cross section (x6.00k).

In the case of the P2 sample taken on the external surface (Fig. 4a), the OM images reveal an uniform beige-grey matrix characterized by fine grains, as well as some parallel rectangular cuts (Fig. 4b). From the morphology point of view, the P2 sample is characterized by coarse grains with straight edges with granular inclusions (Fig. 4c-d).

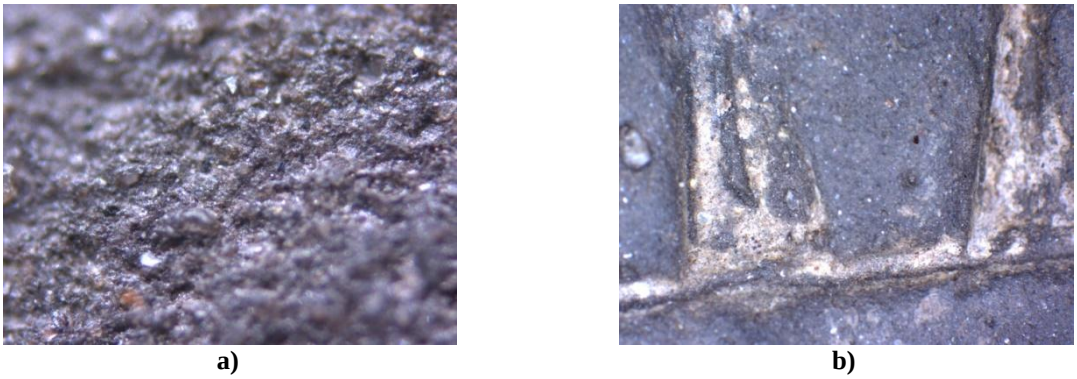

a) **b)**

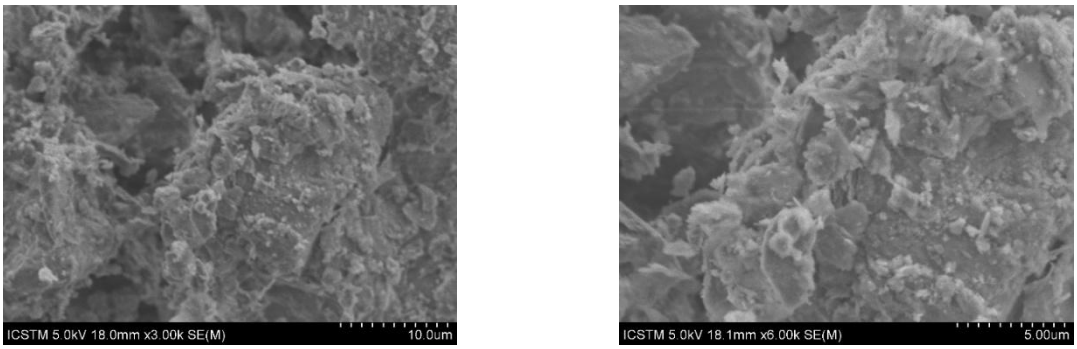

c) **d)**

Figure 4. Ceramic sample P2: a) OM of ceramic fragment (x100); b) OM image of excision (x10); c) SEM image of ceramic in the cross section (x3.00k); d) SEM image of ceramic in the cross section (x6.00k).

The OM image of the P3 sample taken on the external surface (Fig. 5a) reveals an uniform and non-porous black matrix covered by brown deposits; also some triangular excisions, with straight edges, filled with white paste (Fig. 5b) were observed. On the surface of the excisions, some beige-brown deposits were observed. P3 sample's morphology is characterized by grains with round edges with granular inclusions (Fig. 5c-d).

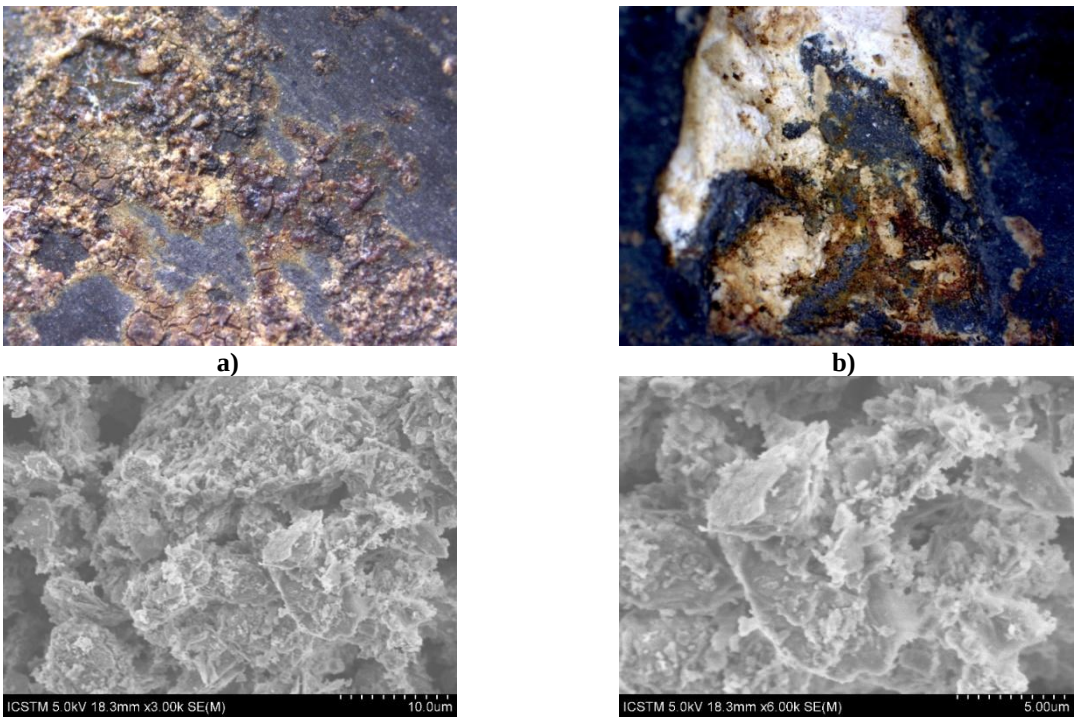

a) **b)**

c) **d)**

Figure 5. Ceramic sample P3: a) OM of ceramic fragment (x40); b) OM image of excision (x10); c) SEM image of ceramic in the cross section (x3.00k); d) SEM image of ceramic in the cross section (x6.00k).

In the case of the P4 sample, the OM images recorded on the external surface (Fig. 6a) reveal an uniform grey-black matrix characterized by fine grains, as well as some triangular excisions (Fig. 6b). From the morphology point of view, this sample is characterized by coarse grains with round edges with few granular or straight edges inclusions (Fig. 6c-d).

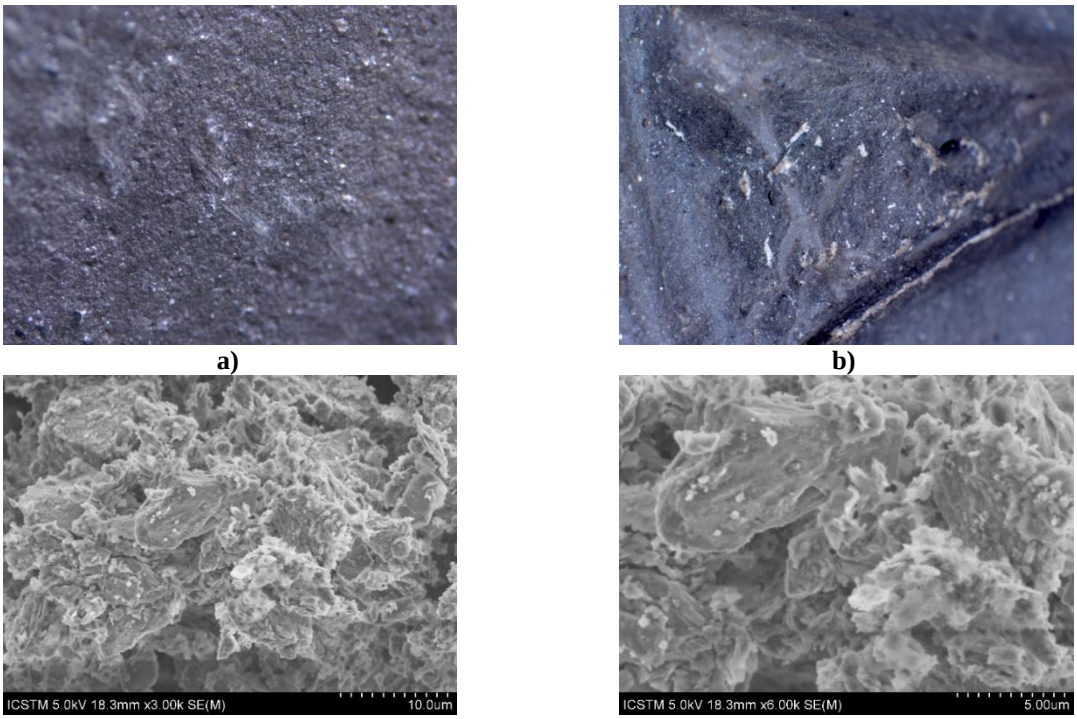

Figure 6. Ceramic sample P4: a) OM of ceramic fragment (x100); b) OM image of excision (x10); c) SEM image of ceramic in the cross section (x3.00k); d) SEM image of ceramic in the cross section (x6.00k).

The OM image of the P5 sample obtained on the external surface (Fig. 7a) reveals an uniform and porous beige matrix with coarse grains, as well as some triangular excisions, with straight edges (Fig. 7b). On the excisions surface, some deep cracks were observed. The morphology images recorded on P5 sample highlight coarse grains with straight edges and granular inclusions (Fig. 7c-d).

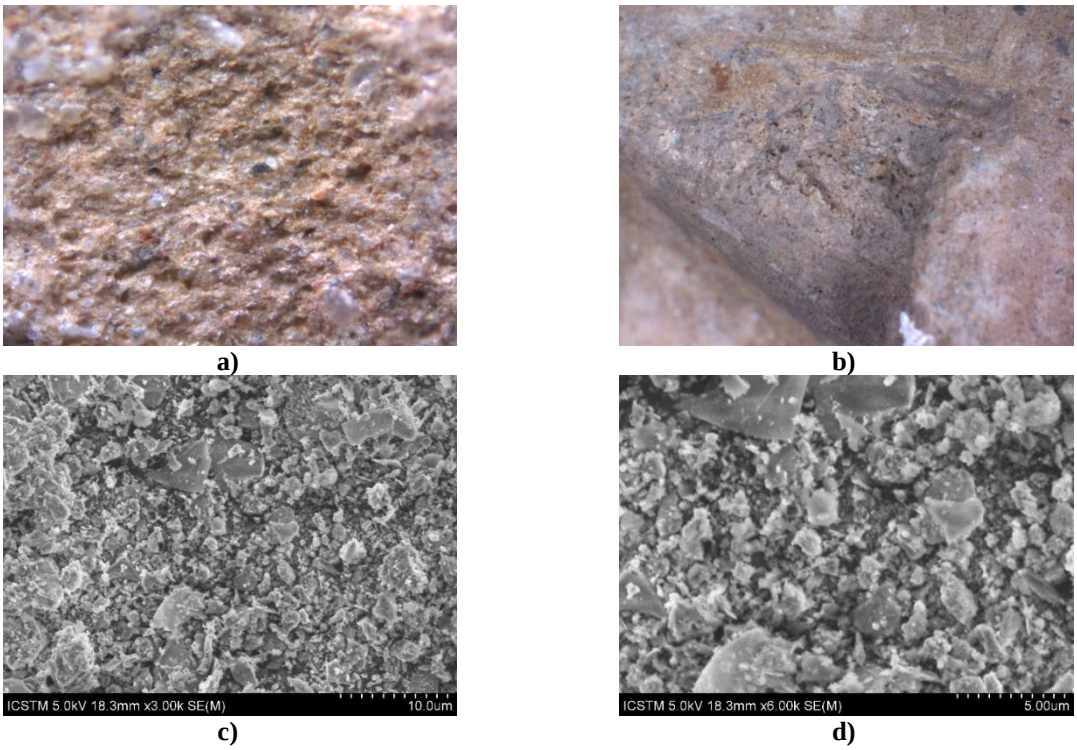

Figure 7. Ceramic sample P5: a) OM of ceramic fragment (x100); b) OM image of excision (x10); c) SEM image of ceramic in the cross section (x3.00k); d) SEM image of ceramic in the cross section (x6.00k).

In the case of the P6 sample, the OM images taken on the external surface (Fig. 8a) show an uniform beige-red matrix characterized by fine grains with triangular excisions made between parallel lines (Fig. 8b). From the morphology point of view, this sample is characterized by coarse grains with straight edges with granular inclusions (Fig. 8c-d).

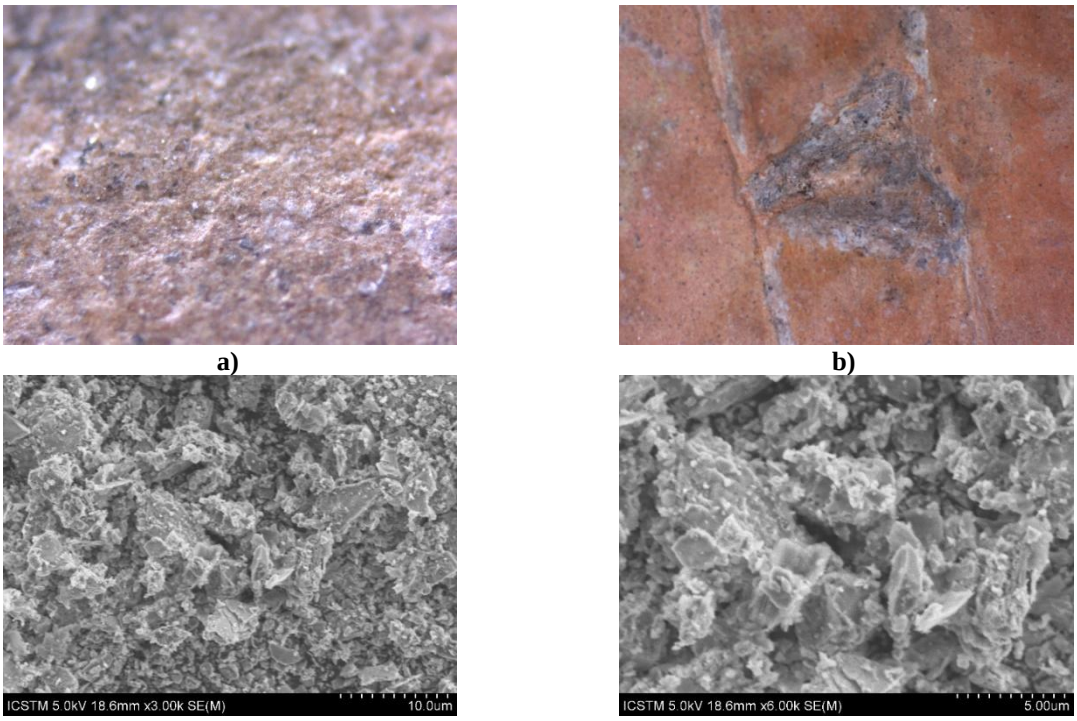

a) **b)** **c)** **d)**

Figure 8. Ceramic sample P6: a) OM of ceramic fragment (x100); b) OM image of excision (x10); c) SEM image of ceramic in the cross section (x3.00k); d) SEM image of ceramic in the cross section (x6.00k).

Considering the OM images of the P7 external surface, the grey-black matrix (Fig. 9a), as well as the triangular excisions, with straight edges (Fig. 9b) can be observed. From the morphology point of view, the P7 sample is characterized by fine grains with round edges, with granular or straight edges inclusions (Fig. 9c-d).

a) **b)**

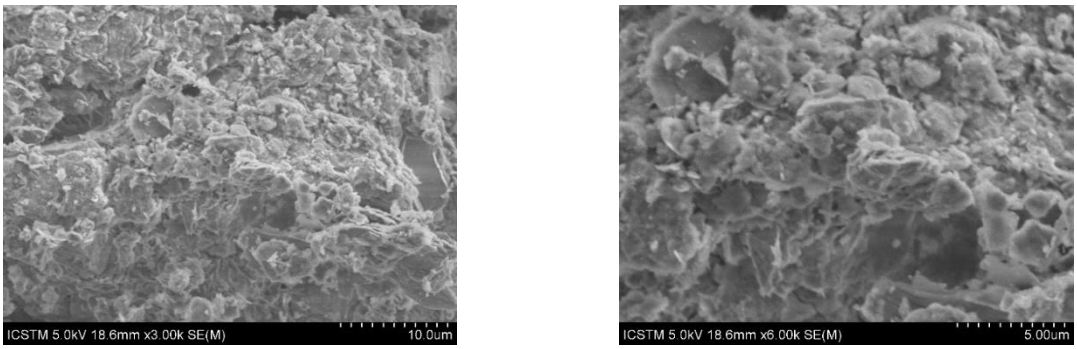

c) **d)**

Figure 9. Ceramic sample P7: a) OM of ceramic fragment (x100); b) OM image of excision (x10); c) SEM image of ceramic in the cross section (x3.00k); d) SEM image of ceramic in the cross section (x6.00k).

The OM image of the P8 sample recorded on the external surface (Fig. 10a) reveals the uniform and porous beige-light brown matrix with fine grains, as well as the triangular excisions (Fig. 10b). This sample is characterized by coarse grains with straight edges with granular inclusions (Fig. 10c-d).

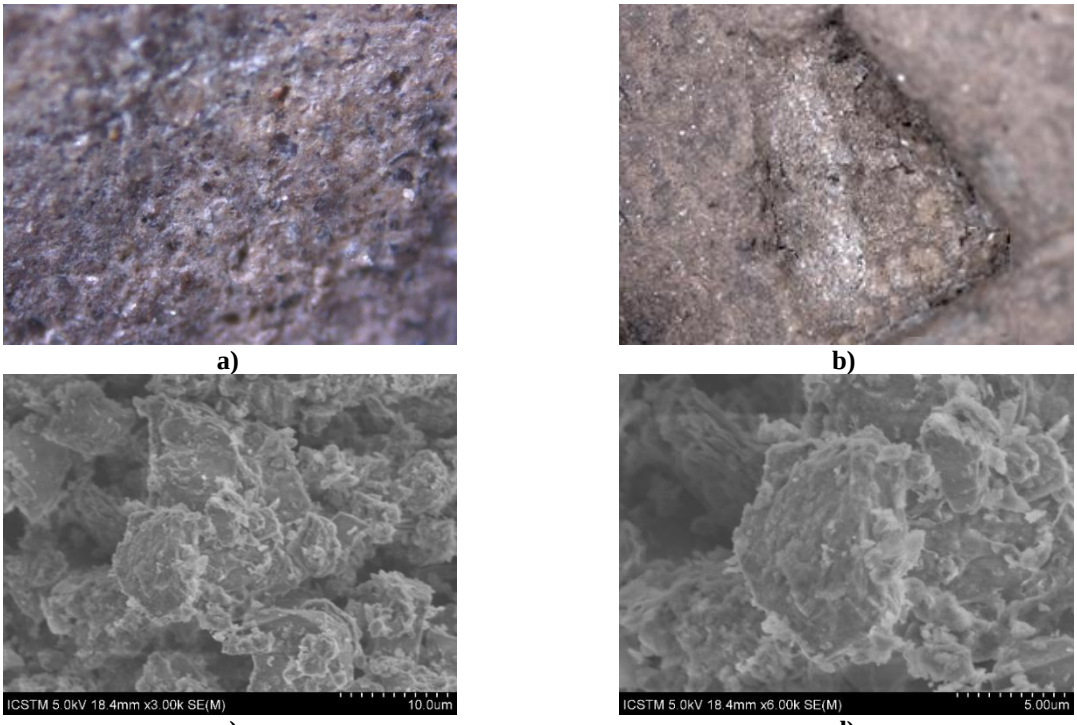

a) **b)**

c) **d)**

Figure 10. Ceramic sample P8: a) OM of ceramic fragment (x100); b) OM image of excision (x10); c) SEM image of ceramic in the cross section (x3.00k); d) SEM image of ceramic in the cross section (x6.00k).

The OM image of the P9 sample taken on the external surface (Fig. 11a) reveals an uniform and porous red matrix with fine grains, as well as, some triangular excisions, with straight edges (Fig. 11b). On the surface of these excisions, some deep cracks were observed. The morphology of P9 sample is characterized by fine grains with round edges - flakes structure similar with clay structure (Fig. 11c-d).

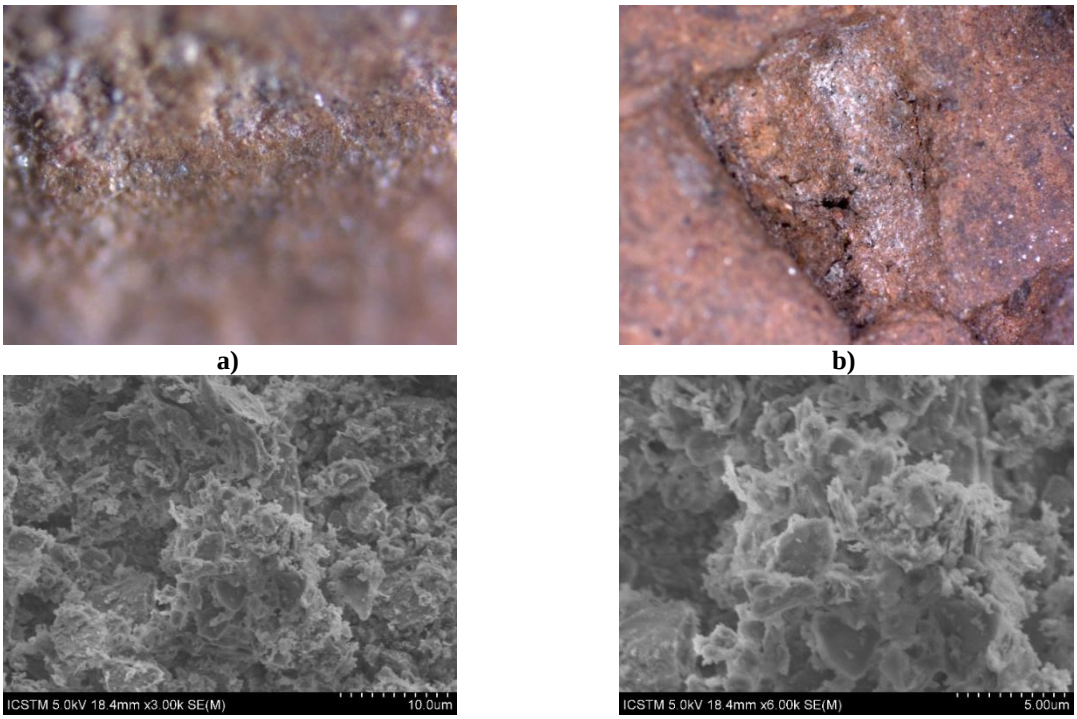

Figure 11. Ceramic sample P9: a) OM of ceramic fragment (x100); b) OM image of excision (x10); c) SEM image of ceramic in the cross section (x3.00k); d) SEM image of ceramic in the cross section (x6.00k).

In the case of the P10 sample, the OM images recorded on the external surface (Fig. 12a) show an uniform beige-grey matrix characterized by fine grains with oval excisions made between parallel straight lines (Fig. 12b). From the morphology point of view, this sample is characterized by fine grains with round edges with few inclusions of grains with straight edges (Fig. 12c-d).

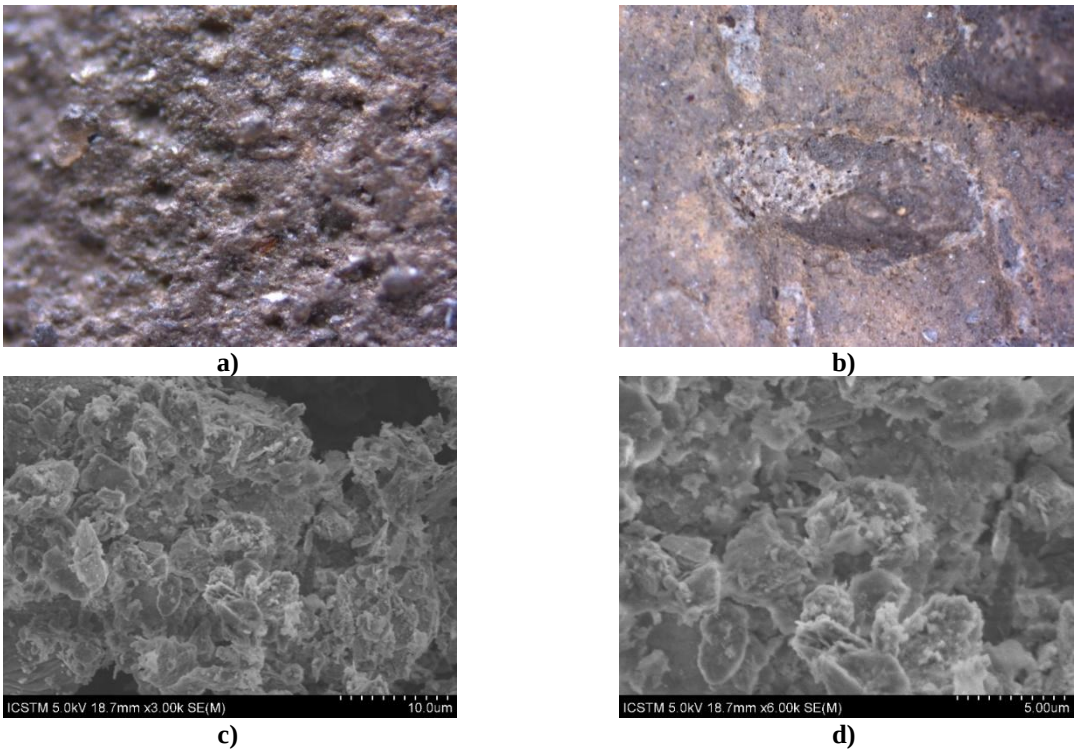

Figure 12. Ceramic sample P10: a) OM of ceramic fragment (x100); b) OM image of excision (x10); c) SEM image of ceramic in the cross section (x3.00k); d) SEM image of ceramic in the cross section (x6.00k).

3.2. ELEMENTAL AND MOLECULAR COMPOSITION

The SEM-EDS method was applied in order to obtain data concerning elemental composition, as well as the source of the raw-materials used for pottery production. The elemental composition of these samples, determined by SEM-EDS, is shown in Table 2. The reported values are expressed in mass percent (wt.%) ± standard deviation (%), normalized to 100 wt.%.

Table 2. The major and minor elements in the studied ceramic fragments, determined by FE-SEM-EDS, expressed in [wt.%±S.D.%] normalized to 100 wt.%.

Sample	Elements								
	C	**O**	**Na**	**Mg**	**Al**	**Si**	**P**	**Fe**	**Ir**
P1	3.25± 0.23	47.12± 2.77	0.57± 0.04	1.77± 0.07	11.71± 0.35	28.39± 1.88	nd*	6.30± 0.43	0.91± 0.07
P2	1.73± 0.13	45.74± 2.35	nd*	1.73± 0.07	13.31± 0.44	28.68± 1.92	nd*	7.62± 0.52	1.20± 0.08
P3	7.70± 0.52	45.38± 2.09	nd*	0.76± 0.03	5.32± 0.04	16.89± 1.14	7.58± 0.53	16.38± 0.87	nd*
P4	2.22± 0.18	48.44± 2.85	0.45± 0.02	1.69± 0.06	13.46± 0.42	29.32± 1.95	nd*	4.44± 0.19	nd*
P5	1.40± 0.09	46.39± 2.57	0.50± 0.02	1.46± 0.04	13.14± 0.40	33.41± 1.98	nd*	3.71± 0.17	nd*
P6	5.44± 0.37	47.90± 2.66	0.32± 0.02	1.82± 0.08	12.73± 0.27	24.63± 1.75	nd*	4.42± 0.18	2.76± 0.12
P7	1.72± 0.09	48.03± 2.80	0.74± 0.05	1.50± 0.05	11.79± 0.19	32.42± 1.95	nd*	3.82± 0.17	nd*
P8	0.95± 0.05	48.35± 2.87	0.46± 0.03	1.44± 0.04	9.94± 0.09	33.01± 1.97	nd*	5.73± 0.32	nd*
P9	0.97± 0.05	47.20± 2.43	nd*	1.54± 0.05	14.04± 0.55	26.95± 1.78	nd*	9.31± 0.69	nd*
P10	2.44± 0.19	45.54± 2.44	nd*	1.06± 0.04	11.62± 0.32	26.86± 1.77	nd*	10.36± 0.71	2.13± 0.10

nd = not detected element or element with value under the limit of detection (LOD≈0.01wt.%).*

The data presented in Table 2 show that the major components in all investigated samples were C, O, Al, Si, and Fe, while elements as Na, Mg, and Ir are minor components. On some EDS spectra, K and Ca were identified, but the content was lower than limit of detection (about 0.01 wt.%). The Na content of 0.3% to 0.6% was detected in six analyzed samples (i.e., P1, P4-P8), whereas in the P1, P2, P6, and P10 samples the concentration of Ir was 0.91% to 2.76%. In addition, the results have shown high concentrations of Al (5.32-14.04%) and Si (16.89-33.41%) which confirm the presence of high content of aluminosilicates – the main components of clay minerals – and quartz [34]. Other elements determined in all samples are Mg (0.76-1.77%) and Fe (3.71-16.38%); the oxides of these elements are typical constituents of clays used for pottery manufacturing [35]. P3 is the only sample with important amounts of P (7.58%); this potsherd has its excision ornamental motifs filled with a white paste (also, with high content of P), and this intriguing topic will be the subject of a future paper.

The chemical composition of ceramic samples obtained by EDS method (Table 2) was correlated with results recorded from ATR-FTIR and Raman spectra. The spectral data of the samples are reported in Tables 3 and 4, in terms of wavenumbers, peak intensity and vibrational assignments. In potsherds recovered from Alba Iulia-Lumea Nouă site, carbonates, silicates / aluminosilicates (i.e., major compounds from kaolin / kaolinites) were identified,

while iron oxides were observed in the recessed areas of edge surface of certain samples (i.e., P6 in FTIR spectrum and for all P1-10 in Raman spectra).

Nonetheless, returning to the ceramic's preparation, regardless of the period, must be emphasized that the clay undergoes thermal transformations in its lattice structure [36-39]. Specifically, at temperature of 400-550°C, clay dehydrates, losing all water molecules. In spite of that, in FTIR spectra of samples, medium / strong intensity peaks of O-H searching / bending vibrations in transmission mode were observed at 3619-3628 cm^{-1} and 3683-3695 cm^{-1}, respectively (Table 3). These hydroxyl absorptions are assigned to kaolin / kaolinite (with interlayer hydrogen bonds in initial structures). That means, in the temperature range of 550-600°C the expulsion of water is reversible (i.e., in a humidity atmosphere, the kaolin will reabsorb water and disintegrate into its fine particulate form). In agreement with the FTIR results, Raman spectra recorded on the ceramic fragments showed weak / medium peaks in the range of 850-807 $cm^{-1,}$ and 1220-1174 cm^{-1}, characteristic of Si–O bend and stretch modes of amorphous glasslike material (Table 4). In FTIR spectra these absorption bands visible in Raman in the range of 1220-807 cm^{-1} are very difficult to identify. In addition, hydrated layered silicates from kaolinite are assimilated with a *double-deck sandwich* in which the water molecules are positioned in various sheets between the silicate anions and interlayer cations. In one of this lattice conformation restricts the direction in which the O-H groups can vibrate. In this case, the O-H groups have a restricted vibration. The hydroxyl stretches for kaolinite show in FTIR spectra as two sharp bands at ca. 3695 and ca. 3619 cm^{-1}, with two slightly smaller bands between 3678 and 3649 cm^{-1} (i.e., P1-10) (Table 3). Carbonates ions showed a strong absorption band from C-O stretching vibrations in the region of 1435-1425 cm^{-1}. Carbonate bending vibrations produce medium intensity band in the region of 878-873 cm^{-1} for the samples P1, P3, P4, and symmetric deformation assigned to the carbonate ion in the region of 713-722 cm^{-1}, for the samples P1-3, P5, P6, and P9, respectively (Table 3).

Table 3. FTIR data in terms of the main groups detected in samples, wavenumbers, peak intensity, and vibrational assignments.

Functional group	Wavenumber [cm^{-1}]	Ceramic fragments (P)										Vibrational assignments [40-44]
		1	2	3	4	5	6	7	8	9	10	
		Peak intensity*										
Carbonate	1425-1435	m	m	m	m	-	m	m	-	-	-	Asymmetric CO_3^{2-} stretching vibration
	873-878	m	-	m	m	-	-	-	-	-	-	Asymmetric CO_3^{2-} bending vibration
	713-722	m	m	m	-	m	m	-	-	m	-	Symmetric deformation of CO_3^{2-}
	360-369	w	s	m	-	s	w	m	-	m	m	C-O stretching vibration
Silicate / aluminosilicate	3690-3695	s	s	s	s	s	s	s	s	s	s	O-H stretching vibration
	3666-3678	w	w	w	w	w	w	w	w	w	w	O-H bending vibration
	3649-3652	w	w	w	w	w	w	w	w	w	w	O-H bending vibration
	3619-3628	s	s	s	s	s	s	s	s	s	s	O-H stretching vibration
	1103 – 1112	m	m	m	m	m	m	m	m	m	m	Si-O stretching vibration
	1028 - 1032	s	s	s	s	s	s	s	s	s	s	Si-O stretching vibration

Table 3. (*continued*)

Functional group	Wavenumber [cm^{-1}]	Ceramic fragments (P)										Vibrational assignments [40-44]
		1	2	3	4	5	6	7	8	9	10	
		Peak intensity*										
Silicate / aluminosilicate	995-1009	s	s	s	-	s	s	s	-	s	s	in-plane Si-O stretching
	795-798	m	m	m	w	m	m	m	m	m	m	Si-O-Al stretching vibration
	774-779	s	s	s	m	s	s	s	m	m	m	Si-O-Al stretching vibration
	755 - 789	w	w	w	w	w	w	w	w	w	w	Si – O stretching vibration
	693-694	m	m	m	m	m	m	m	m	m	m	Si-O stretching vibration
	441-451	w	w	w	w	w	w	w	w	w	w	Si-O-Al bending vibration
	424-428	m	w	w	m	w	w	-	w	w	-	Si-O-Al bending vibration
	390-395	w	m	w	m	w	m	m	w	m	m	Si-O band / Fe-O band
	355-359	w	s	s	m	m	s	m	w	m	m	Si-O bending vibration
Iron oxide	667-671	m	m	w	-	w	-	-	-	-	-	Fe-O / Al - O band
	532-536	-	w	-	-	-	w	-	-	-	-	Fe-O band / Si-O-Al
	557	-	-	-	-	-	w	-	-	-	-	Fe-O band

* *w=weak, m=medium, s=strong.*

In the FTIR and Raman spectra recorded of the sample edges (Tables 3 and 4), the weak broad band present around 667 cm^{-1} is characteristic to iron oxide compounds (i.e., spinel iron(II,III) oxide, $Fe^{2+}Fe^{3+}{}_2O_4$ called usually magnetite and iron(III) oxide, α-Fe_2O_3 known as hematite). The presence of both iron ions (i.e., $Fe^{2+}Fe^{3+}$) in magnetite is due to an incomplete phase transformation during firing, most likely in oxidizing atmosphere [45]. It is well known that the magnetite converts to maghemite (i.e., Fe(II)-deficient magnetite, with formula γ-Fe_2O_3) at low-temperature oxidation of spinel containing iron(II) such as magnetite (e.g., 200°C) and finally, by increasing the temperature at 400 °C, hematite is obtained [36, 45]. On the other hand, it should be highlighted that the transformation process of maghemite into hematite is a result of previous heat treatments achieved by the people from antiquity as well as due to the aluminum ions presence or other ions [46-48]. Bending vibrations for Si-O from silicates occured below 600 cm^{-1} according to both FTIR and Raman investigation (Tables 3 and 4).

Table 4. Raman data in terms of the main groups detected in samples, wavenumbers, peak intensity, and vibrational assignment.

Functional group	Raman shift [cm^{-1}]	Ceramic fragments (P)										Vibrational Assignments [49-52]
		1	2	3	4	5	6	7	8	9	10	
		Peak intensity*										
Carbonates	1421-1451	w	-	m	w	w	w	w	w	w	w	Asymmetric CO_3^{2-} stretching of $CaCO_3$
	875-879	w	w	m	w	m	w	w	w	w	w	Asymmetric CO_3^{2-} bending of $CaCO_3$
Silicate / aluminosilicate	1630-1639	m	w	w	-	w	w	w	w	-	w	O-H bending
	1220-1253	w	w	w	w	w	w	w	w	w	w	Si-O bend and stretch modes of amorphous glasslike material
	1174-1198	w	w	w	w	w	w	w	w	w	w	Si-O bend and stretch modes of amorphous glasslike material

Table 4. (*continued*)

Functional group	Raman shift [cm^{-1}]	Ceramic fragments (P)										Vibrational Assignments [49-52]
		1	2	3	4	5	6	7	8	9	10	
		Peak intensity*										
Silicate / aluminosilicate	1118-1126	w	w	w	w	w	w	w	w	w	w	Si-O bend and stretch modes of amorphous glasslike material
	1101-1109	m	m	m	m	m	m	m	m	m	m	Si – O stretching vibration
	807-850	w	w	w	w	w	m	m	m	m	m	Si-O bend and stretch modes of amorphous glasslike material
	795-798	-	m	w	-	-	-	-	-	-	-	Si-O stretching vibration
	774-780	w	w	-	-	w	-	-	-	-	w	Si-O stretching vibration
	763-772	w	-	s	m	w	w	w	w	w	w	Al-O-Si stretching vibration
	693-694	m	m	m	w	m	w	w	m	m	m	Si-O stretching vibration
	655-673	-	w	-	-	w	m	w	m	w	m	Al-Si-O stretching vibration
	480-498	-	w	m	m	w	w	w	w	w	w	Si-O bending vibration
	441-451	m	m	w	w	m	s	w	m	m	m	Si-O bending stretching
	424-428	-	m	-	-	w	w	w	w	w	w	Si-O-Al stretching vibration
	390-395	m	s	m	m	s	m	m	m	s	m	Si-O bending vibration
	355-359	w	w	w	w	w	w	w	w	w	w	Si-O bending vibration
Iron oxide	667-671	-	-	-	-	w	-	-	-	-	w	Fe-O band
	552	-	-	-	-	-	w	-	-	-	-	Fe-O band
	384-393	-	m	s	-	w	m	m	m	s	m	Fe-O-Fe band
	305-315	m	s	s	s	s	m	m	m	m	m	Fe-O band

* *w=weak, m=medium, s=strong;* ** *Centenoa et al. 2012; Palanivel and Velraj 2007; Partyka and Lesniak 2016; Saikia et al. 2016.*

The firing temperatures were estimated (predicted) using SEM and FTIR data, according to Velraj et al. [18, 19], as function of clay type (i.e., calcareous or non-calcareous), vitrification stage, as well as, the presence of 875 and 535 cm^{-1} bands. The values for firing temperatures are shown in Table 5.

Table 5. Firing temperatures predicted by both SEM and FTIR methods

Sample	Colour	Atmosphere	Clay type (1)	Vitrification stage (2)	Firing temperature predicted by SEM [°C]	Band 875 cm^{-1} (3)	Band 535 cm^{-1} (3)	Firing temperature predicted by FTIR [°C]	Firing temperature [°C]
P1	Mixed	Oxidizing	NC	IV	800-850	S	NS	>800	800-850
P2	Mixed	Oxidizing	NC	NV	<800	NS	S	>600	600-800
P3	Black	Reducing	NC	IV	800-850	S	NS	>800	800-850
P4	Black	Reducing	NC	IV	800-850	S	NS	>800	800-850
P5	Red	Oxidizing	NC	NV	<800	NS	NS	<600	500-600
P6	Red	Oxidizing	NC	IV	800-850	NS	S	>600	800-850
P7	Black-topped	Oxidizing	NC	NV	<800	NS	NS	<600	500-600
P8	Red	Oxidizing	NC	NV	<800	NS	NS	<600	500-600
P9	Red	Oxidizing	NC	NV	<800	NS	NS	<600	500-600
P10	Red	Oxidizing	NC	NV	<800	NS	NS	<600	500-600

(1) Calcareous (C) / Non-calcareous (NC); (2) Unobserved Vitrification (NV) / Initial Vitrification (IV) stage; (3) with signal (S) / without signal (NS).

The firing temperatures were predicted based on the fact that some IR bands appear or disappear at fixed values of temperature: band at 915 cm^{-1}, corresponding to Al(OH) vibrations, disappears at 500°C; band at 875 cm^{-1}, corresponding to asymmetric CO_3^{2-} bending of $CaCO_3$, indicates that the ceramic fragment was fired above 800°C; band at 535 cm^{-1} corresponding to Fe-O (hematite), indicates that the ceramic fragment was fired above 600°C [18, 19, 53]. Taking into account the above explanations, the analyzed samples can be

grouped in 3 classes: 800-850°C (P1, P3, P4, and P6), 600-800°C (P2) and 500-600°C (P5, P7-P10).

3.3. DATA PROCESSING

Based on the mean values for each element determined in ceramic fragments by SEM-EDS, the Pearson's correlations were achieved. Correlation analyzes were performed to determine the relationships between the chemical elements. The statistical significance and validity of the relationships were verified by using test statistics. The coefficient of determination (R^2) is the proportion of variation of the dependent variable, which can be predicted from the independent variable. Higher values of R^2 correspond to a stronger relationship between dependent and independent variables. The Pearson's correlations (R) of chemical elements determined in the ceramic fragments are presented in Table 6.

Table 6. Pearson's correlations (Pc) of chemical elements determined in the ceramic fragments.

Correlations[c]										
		C	O	Na	Mg	Al	Si	P	Fe	Ir
C	Pc	1	-0.328	-0.264	-0.420	-0.691*	-0.880**	0.794**	0.576	0.286
	Sig. (2-tailed)		0.355	0.461	0.227	0.027	0.001	0.006	0.081	0.422
O	Pc		1	0.686*	0.591	0.340	0.493	-0.485	-0.703*	-0.189
	Sig. (2-tailed)			0.028	0.072	0.336	0.147	0.155	0.023	0.600
Na	Pc			1	0.429	0.168	0.637*	-0.379	-0.758*	-0.277
	Sig. (2-tailed)				0.216	0.643	0.048	0.280	0.011	0.439
Mg	Pc				1	0.774**	0.517	-0.752*	-0.792**	0.205
	Sig. (2-tailed)					0.009	0.126	0.012	0.006	0.571
Al	Pc					1	0.609	-0.883**	-0.704*	0.194
	Sig. (2-tailed)						0.061	0.001	0.023	0.591
Si	Pc						1	-0.806**	-0.827**	-0.243
	Sig. (2-tailed)							0.005	0.003	0.498
P	Pc							1	0.815**	-0.239
	Sig. (2-tailed)								0.004	0.506
Fe	Pc								1	-0.036
	Sig. (2-tailed)									0.920
Ir	Pc									1
	Sig. (2-tailed)									

** Correlation is significant at the 0.05 level (2-tailed); ** Correlation is significant at the 0.01 level (2-tailed); [c] Listwise N=10*

In the case of ceramic samples, the positive correlation/ dependence between C and P (R=0.794), even if there is also a dependency relationship between C and Fe (R=0.576), the value of Sig. is > 0.05 which prevents from stating that the result is statistically significant for the analyzed sample. There is also a positive dependence relationship between Mg and Al (R=0.774), meanwhile between Al and P there is an inversely proportional dependence relationship (R=-0.883). Statistically significant, inverse dependence relationships are also between Fe and Mg (R=-0.792) or between Fe and Si (R=-0.827). The relationship between P and Fe is a positive dependence (R=0.815).

Taking into account the elemental content of clays (collected from the area), reported in previous article [10], the similarity relationship between ceramic fragments and clays, as well as the cluster analysis were performed. In order to predict a similarity relationship

between the chemical elements of the ceramic fragments and the clay, their average values (obtained as it is described in Subsection 2.3 – Data processing) were used.

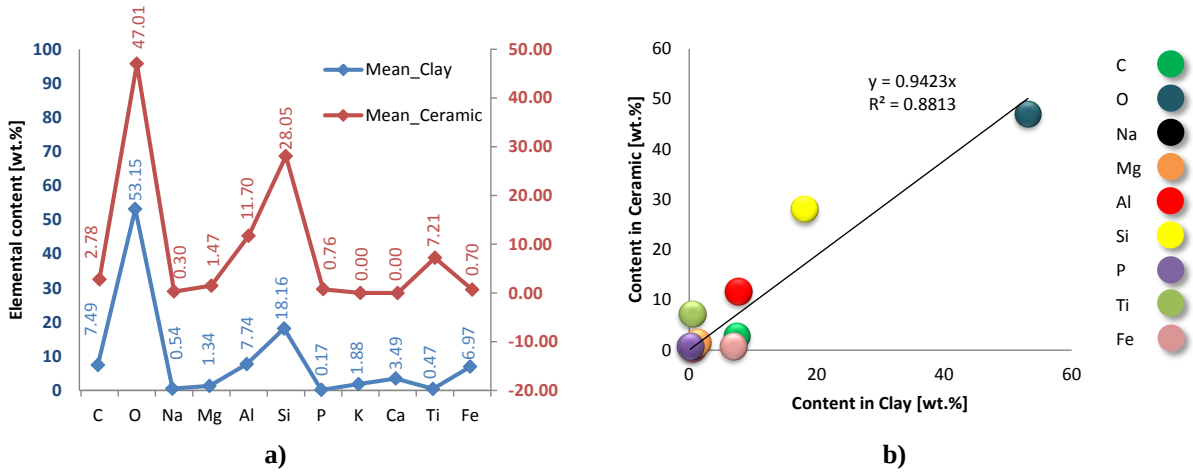

Figure 13. Analysis of the similarity relationship between the chemical composition of the ceramic and clay samples: a) mean values of elements (similar variations except Ti and Fe); b) linear correlation between elements in clay and elements in ceramic.

Fig. 13a shows the variations of chemical elements present in clay and ceramic fragments. Both types of materials (clay and ceramic) have similar variations except Ti and Fe. It is noteworthy that the mean values for Al, Si and Ti are higher in ceramic samples than in clay and this can be explained by the fact that some sand was added in clay to increase the resistance to firing. The same observation is highlighted in Fig. 13b by the presence of these elements above the drawn trend-line.

The Principal Component Analysis (PCA) by component plot in rotated space methods was used to identify the similarity between ceramic fragments. After factors rotation, two principal components were confirmed through PCA typical graphic representation. These two components (PC1 and PC2) are represented in Fig. 14a. The values of the correlation coefficients (from matrix generated in the first step) are coordinates of the initial variables in the vectorial plan of the two principal components [30].

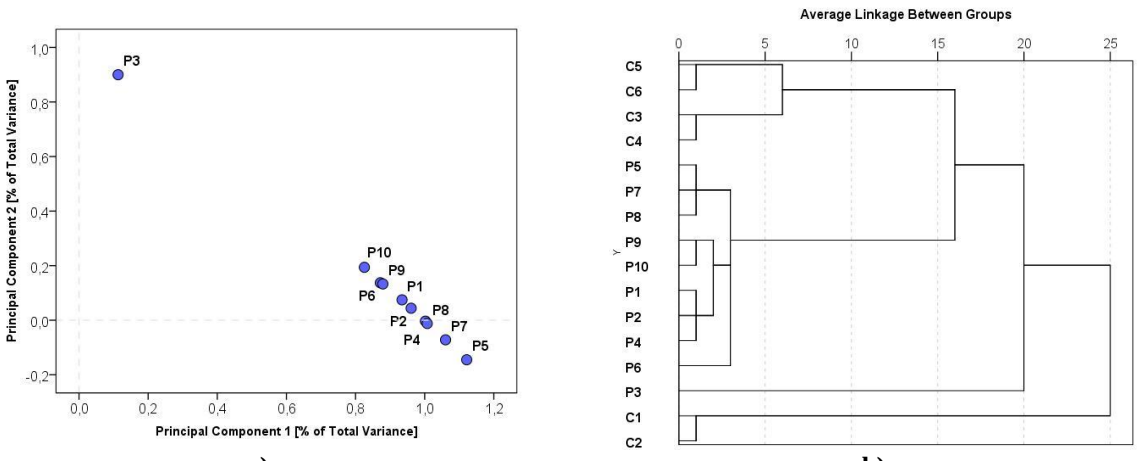

Figure 14. Statistical analyses: a) Principal Component Analysis (PCA) – Component plot in rotated space of ceramic fragments; b) Cluster analysis (dendrogram) of clay and ceramic samples obtained by IBM SPSS Statistics 21 (Average Linkage method).

Fig. 14a shows a good similitude between samples (except P3), with PC1 values between 0.990 and 0.999 and PC2 ranged from -0.133 to 0.037. The P3 samples is characterized by PC1=0.916 and PC2=0.399. It is obvious that this sample is not very similar with the other nine samples from elemental composition point of view.

The cluster analysis is usually used to classify objects with similar characteristics (i.e., chemical profile) in groups or classes. In this study, this type of statistical analysis was used to establish if the clay samples (collected from archaeological site or around) represents the main source for ceramic manufacturing and thus, if the ceramic is made locally or taken from other areas. Using the elemental compositions of ceramic fragment (data presented in this study) and clay (data reported by Bintintan et al. [10]), the dendrogram through Average Linkage method was achieved (Fig. 14b).

Taking into account the differences in elemental content of ceramic fragments, the cluster analysis was expected to group the samples under multiple classes. However, the dendrogram reveals that: 9 ceramic fragments (except P3) out of all analyzed samples belong to the same group, with a strong correlation between them. Moreover, a strong correlation between the cluster of the 9 ceramic and 4 clay samples (C3-C6) was highlighted. This can confirm that these 9 ceramic samples belong to vessels locally made, while P3 samples can be considered as imported from elsewhere or obtained through mixing clay with some existent minerals in the area during the process of ceramic manufacturing.

4. CONCLUSIONS

First of all, from the archaeometric point of view, along with other older or recent papers [14, 53-55], this research contributes to deciphering the craft of Neolithic potters from the present-day territory of Transylvania. The main contribution of this study is that it shows both possible local production of Precucuteni-type pottery discovered at Alba Iulia-*Lumea Nouă* site which seems to be attested throughout its use, and the presence of one single import with identifiable provenance. The previous analyses mentioned by Bintintan et al. [14, 15], concluded that the Eneolithic potters from Alba Iulia-*Lumea Nouă* used local clays in pottery production. The use of reducing firing and the black-topped technique (Fig. 1a: P4, P7), both specific to the Foeni group [7, 56], is an additional argument indicating the local production for the ceramics studied in this article.

Therefore, the presence of an import within a small sample may suggest that there were in fact more imports than was initially suspected, based on macroscopic observations, a finding that would be consistent with the proven links between the Neolithic and Eneolithic communities from Transylvania and neighboring regions [5, 7]. In this respect, we noticed that P3 sample displays excised ornaments filled with white paste in a similar technique as the Precucuteni pottery from the region of Moldova [2, 3, 8].

The most significant result of this study regards the provenance of the pottery referring to the integration of analytical data with archaeological/statistical observations in order to prove the similarity relationship between pottery and local/regional clay, specifically to establish the clay source/provenance of this kind of pottery. In this respect, non-invasive / micro-destructive techniques (*i.e.*, OM, FE-SEM-EDS, ATR-FTIR, and Raman spectroscopy) and statistical analysis were used, as also for providing more comprehensive information about the studied fragments. In addition, morphological and chemical analyses were overlapped to predict the firing temperature, and also to evaluate the Pearson's correlations between chemical elements.

Acknowledgements: *This work is supported by project POCU 125040, entitled "Development of the tertiary university education to support the economic growth - PROGRESSIO", co-financed by the European Social Fund under the Human Capital Operational Program 2014-2020 (for Diana Elena Tomus (Szabo)) and by the project 51PCCDI/2018, financed by Romanian National Authority for Scientific Research (UEFISCDI) "New diagnosis and treatment technologies for the preservation and revitalization of archaeological components of the national cultural heritage".*

REFERENCES

[1] Marinescu-Bilcu, S., Cultura Precucuteni în Câmpia Moldovei / Precucuteni culture in Moldovei Plain. In *Din trecutul județului Botoșani*, Muzeul Judetean Botosani: Botosani, pp.49-53, 1974.
[2] Garvan, D., *Contribuții la cunoașterea culturii Precucuteni* / Contributions to the knowledge of the Precucuteni culture, Editura Constantin Matasă, Piatra Neamt, 2013.
[3] Marinescu-Bilcu, S., *Cultura Precucuteni pe teritoriul României* / Precucuteni culture on the Romanian territory, Editura Academiei Republicii Socialiste România, Bucharest, 1974.
[4] Lazarovici, G., Lazarovici, C.M., *Analele Banatului*, **XXIV**, 37, 2016.
[5] Gligor, M., *Plural*, **5**(1), 164, 2017.
[6] Gligor, M., *Apulum*, **46**, 233, 2009.
[7] Gligor, M., *Aşezarea neolitică şi eneolitică de la Alba Iulia-Lumea Nouă în lumina noilor cercetări* / Neolithic and Eneolithic settlement from Alba Iulia-Lumea Nouă in the light of recent research, Editura Mega, Cluj-Napoca, 2009.
[8] Ursu, C.E, Aparaschivei, C., *Brukenthal Acta Musei*, **IX**(1), 19, 2014.
[9] Roska, M., *A Torma Zsófia-Gyüjtemény. Az Erdély nemzeti múzeum érem-és régiségtárában* / The Torma Zsófia Collection. In the numismatic-archaeological department of the Transylvanian National Museum, Minerva Irodalmi Es Nyomdai Műintézet Rt., Kolozsvar (Cluj-Napoca), 1941.
[10] Bintintan, A., Gligor, M., Dulama, I.D., Teodorescu, S., Stirbescu, R.M., Radulescu, C., *Revista de Chimie*, **68**(4), 847, 2017.
[11] Ion, R.M., Nyokong, T., Nwahara, N., Suica-Bunghez, I.R., Iancu, L., Teodorescu, S., Dulama, I.D., Stirbescu, R.M., Gheboianu, A., Grigorescu, R.M., Wood preservation with gold hydroxyapatite system. *Heritage Science*, **6**, 37, 2018.
[12] Ion, R.M., Tincu, S., Ion, N., Bucurica, I.A., Teodorescu, S., Dulama, I.D., Stirbescu, R.M., Gheboianu, A.I., Radulescu, C., Ion, M.L., Iancu, L., Grigorescu, R.M., *Romanian Reports in Physics*, **71**(3), 804, 2019.
[13] Ion, R.M., Bakirov, B.A., Kichanov, S.E., Kozlenko, D.P., Belushkin, A.V., Radulescu, C., Dulama, I.D., Bucurica, I.A., Gheboianu, A.I., Stirbescu, R.M., Teodorescu, S., Iancu, L., David, M.E., Grigorescu, R.M., *Applied Science*, **10**(11), 3781, 2020.
[14] Bintintan, A., Gligor, M., Dulama, I.D., Radulescu, C., Stihi, C., Ion R.M., Teodorescu, S., Stirbescu, R.M., Bucurica, I.A., Pehoiu, G., *Romanian Journal of Physics*, **64**(5-6), 903, 2019.
[15] Bintintan, A., Gligor, M., Radulescu, C., Dulama, I.D., Olteanu, R.L., Teodorescu, S., Stirbescu, R.M., Bucurica, I.A., *Analytical Letters*, **52**(15), 2348, 2019.
[16] Freitas, R.P., Coelho, F.A., Felix, V.S., Pereira, M.O., Torres de Souza, M.A., Anjos, M.J., *Spectrochimica Acta A*, **193**, 432, 2018.

[17] Brambilla, L., Caiazzo, C.F., Michel, A., Mischler, S., Bertholon, R., *Measurement*, **127**, 256, 2018.
[18] Velraj, G., Janaki, K., Mohamed Musthafa, A., Palanivel, R., *Spectrochimica Acta A*, **72**, 730, 2009.
[19] Velraj, G., Tamilarasu, S., Ramya, R., *Materials Today: Proceedings*, **2**, 934, 2015.
[20] Bolewski, A., Matosz, M., Pohorecki, W., del Hoyo-Meléndez, J.M., *Radiation Physics and Chemistry*, **171**, 108699, 2020.
[21] Smith, G.D., Clarck, R.J.H., Raman microscopy in art history and conservation science. *Studies in Conservation*, **46**, 92, 2001.
[22] Vandenabeele, P., Tate, J., Moens, L., *Analytical and Bioanalytical Chemistry*, **3**(387), 813, 2007.
[23] Hussein, A.M., Madkour, F.S., Afifi, H.M., Abdel-Ghani, M., Abd Elfatah, M., *Vibrational Spectroscopy*, **106**, 102987, 2020.
[24] Masi, G., Balbo, A., Esvan, J., Monticelli, C., Avila, J., Robbiola, L., Bernardi, E., Bignozzi, M.C., Asensio, M.C., Martini, C., Chiavari, C., *Applied Surface Science*, **33**, 468, 2018.
[25] Hubin, A., Terryn, H., X-ray photoelectron and Auger electron spectroscopy. In *Comprehensive Analytical Chemistry, Vol. XLII - Non-Destructive Microanalysis of Cultural Heritage Materials*; Janssens, K., Van Grieken, R. (Eds.), Elsevier, Amsterdam, pp. 277-312, 2004.
[26] Festa, G., Andreani, C., Arcidiacono, L., Grazzi, F., Senesi, R., Neutron Diffraction and (n, γ)-Based Techniques for Cultural Heritage. In *Advanced Nanomaterials - Nanotechnologies and Nanomaterials for Diagnostic, Conservation and Restoration of Cultural Heritage*; Lazzara, G., Fakhrullin, R. (Eds.), Elsevier, Amsterdam, pp. 61-77, 2019.
[27] Khaweerat, S., Ratanatongchai, W., Wonglee, S., Schillinger, B., *Physics Procedia*, **88**, 123, 2017.
[28] Sister Serafima, Duliu, O.G., Manea, M.M., Vasilica, S., Radulescu, C., Constantinescu, B., Stan, D., Culicov, O.A., Zincovscaia, I., *Microchemical Journal*, **150**, 104126, 2019.
[29] Georgescu, A.A., Eliescu, A., Nicolescu, C.M., Bumbac, M., Cioatera, N., Mureseanu, M., Buruleanu, L.C., *Analytical Letters*, **52**(13), 2007, 2019.
[30] Radulescu, C., Buruleanu, L.C., Georgescu, A.A., Dulama, I.D., Correlation between Enzymatic and Non-Enzymatic Antioxidants in Several Edible Mushrooms Species. In *Food Engineering*; Coldea, T.E. (Ed.), IntechOpen, London, pp. 1-31, 2019.
[31] Stanescu, S.G., Danila, A., Horga, M.G., *Journal of Science and Arts*, **18**(1), 159, 2018.
[32] Pehoiu, G., Murarescu, O., Coman, D.M., Stanescu, S.G., Coman, M.D., *Journal of Science and Arts*, **18**(2), 489, 2018.
[33] Radulescu, C., Olteanu, R.L., Stihi, C., Florescu, M., Stirbescu, R.M., Stanescu, S.G., Nicolescu, C.M., Bumbac, M., *Journal of Chemometrics*, **34**(6), e3234, 2020.
[34] Bleam, W., Clay Mineralogy and Chemistry. In *Soil and Environmental Chemistry*, 2nd ed. Bleam, W. (Ed.), Elsevier, Amterdam, pp. 87-146, 2017.
[35] Chukhrov, F.V., Gorshkov, A.I., Rudnitskaya, E.S., Beresovskaya, V.V., Sivtsov, A.V., *Clays and Clay Minerals*, **28**(5), 346, 1980.
[36] Derrick, M.R., Stulik, D., Laundry, J.M., *Infrared Spectroscopy in Conservation Science. Scientific Tools for Conservation*, The Getty Conservation Institute, Los Angeles, 1999.
[37] Mangone, A., Giannossa, L.C., Colafemmina, G., Laviano, R., Traini, A., *Microchemical Journal*, **92**, 97, 2009.
[38] Bumbac, M., Serban, B., Luca, C., Nechifor, G., Voicu, S., *Revista de Chimie*, **57**(9), 927, 2006.

[39] Dumitrescu, C., Olteanu, R.L., Bumbac, M., Gorghiu, L.M., *Revista de Chimie*, **60**(4), 329, 2009.
[40] Vankatachalapathy, R., Manoharan, C., Dhanapandian, S., Sundareswaran, T., Deenadayalan, K., *Journal of Current Sciences*, **5**(2), 695, 2004.
[41] Ravisankar, R., Kiruba, S., Eswaran, P., Senthilkumar, G., Chandrasekaran, A., *Journal of* Chemistry, **7**(S1), S185, 2010.
[42] Arokem, U.O., Abdulkarim, A., Ogubunka, R.O., *ATBU Journal of Environmental Technology*, **6**(1), 42, 2013.
[43] Oancea, A.V., Bodi, G., Nica, V., Ursu, L.E., Drobota, M., Cotofana, C., Vasiliu, A.L., Simionescu, B.C., Olaru, M., *Journal of the European Ceramic Society*, **37**(15), 5079, 2017.
[44] Lettieri, M., Giannotta, M.T., *International Journal of Experimental Spectroscopic Techniques*, **2**, 009, 2017.
[45] de Faria, D.L.A., Silva, S.V., de Oliveira, M.T., *Journal of Raman Spectroscopy*, **28**(11), 873, 1997.
[46] Jing, G., Di, Z., Lu, W., Hong, W., Tao, S., Qi, Z.M., Xi, Y., *Dalton Transactions*, **42**(5), 1483, 2013.
[47] Xiao, E.C., Cao, Z., Li, J., Li, X.H., Liu, M., Yue, Z., Chen, Y., Chen, G., Song, K., Zhou, H., *Journal of the American Ceramic Society*, **103**, 2528, 2020.
[48] Šupová, M., *Ceramics International*, **41**, 9203, 2015.
[49] Saikia, B.J., Parthasarathy, G., Borah, R.R., Borthakur, R., *International Journal of Geosciences*, **7**, 873, 2016.
[50] Palanivel, R., Velraj, G., *Indian Journal of Pure & Applied Physics*, **45**, 501, 2007.
[51] Partyka, J., Leśniak, M., *Spectrochimica Acta A*, **152**, 82, 2016.
[52] Centenoa, S.A., Williams, V.I., Little, N.C., Speakman, R.J., *Vibrational Spectroscopy*, **58**, 119, 2012.
[53] Enea-Giurgiu, A., Ionescu, C., Hoeck, V., Tamas, T., Roman, C., *Clay Miner*als, **54**(3), 255, 2019.
[54] Goleanu, A., Marian, A., Florescu, C., Gligor, M., Varvara, S., *Revue Roumaine de Chimie*, **50**(11-12), 939, 2005.
[55] Varvara, S., Fabbri, B., Gualtieri, S., Ricciardi, P., Gligor, M., *Studia Universitatis Babes-Bolyai Series Chemia*, **LIII**(1), 5, 2008.
[56] Bintintan, A., Gligor, M., *Studia Antiqua et Archaeologica*, **XXI**(1), 5, 2016.